

# Model of collimated jets with high energy particles

C. Barbachoux<sup>1,2\*</sup>, J. Gariel<sup>1†</sup>, G. Marcilhacy<sup>1‡</sup> and N. O. Santos<sup>1,3§</sup>

<sup>1</sup> LERMA-UPMC, Université Pierre et Marie Curie, Observatoire de Paris, CNRS, UMR 8112, 3 rue Galilée, Ivry sur Seine 94200, France.

<sup>2</sup> Université de Nice Sophia Antipolis, Institut Non Linéaire de Nice, UMR CNRS 6618, 1361 route des Lucioles, 06 560 Valbonne, France.

<sup>3</sup> School of Mathematical Sciences, Queen Mary, University of London, Mile End Road, London E1 4NS, U. K.

## Abstract

**Context** The increasing data set of precise observations of very energetic and collimated jets, with black hole (BH) as putative central engine, at different astrophysical scales and in various environments, should soon permit to discriminate and classify current theoretical models able to describe the jets formation.

**Aims** Constructing a purely gravitational theoretical model of perfectly collimated jets of high energy particles in the ideal case where the central engine is a Kerr BH of mass  $M$  and angular momentum by unit of mass  $a$ .

**Methods** Studying in Weyl coordinates  $(\rho, z)$  the unbound Kerr 2D-geodesics which are asymptotes to straight lines parallel to the  $z$  axis of equations

$$\rho = \text{constant} \equiv \rho_1 = \left[ \left( \frac{a}{M} \right)^2 + \frac{\mathcal{Q}}{E^2 - 1} \right]^{1/2},$$

of which existence was recently demonstrated (Gariel et al.,2010). On these geodesics, flow test particles of energy  $E$ , with a Carter constant  $\mathcal{Q}$  and (necessarily) an angular momentum  $L_z = 0$ .

**Results** We express the motion constants  $E$  and  $\mathcal{Q}$  as functions of  $r_1$  and  $r_2$ , which are real roots of characteristics of the geodesics equations

---

\*cecile.barbachoux@obspm.fr

†jerome.gariel@upmc.fr

‡gmarcilhacy@hotmail.com

§nilton.santos@upmc.fr and N.O.Santos@qmul.ac.uk

system. In the special case of a double root  $r_1 = r_2 = Y$ , and, as an example, fixing  $a = M/2$ , the  $Y$  parametrization of the constants  $E$  and  $\rho_1$  displays the following properties: 1) When  $E \rightarrow \infty$  it implies  $|\mathcal{Q}| \rightarrow \infty$ , but  $\rho_1$  remains finite and tends to only two possible values,  $\rho_1/\rho_e = 10.241$  and  $0.69$  with  $\rho_e = a/M$ . 2)  $E$  steeply decreases from infinity to small values, while  $\rho_1$  concomitantly varies little inside two narrow ranges of  $\rho_1/\rho_e$ :  $[10.241; 10.65]$  and  $[0.69; 0.67]$ . Thus, the jet has a radial structure. Hence, the energy flux can be calculated. Furthermore, based on observed data of the jets powers, we can obtain the mean particles density, the particles flow, the speed and the Lorentz factor of the jets, for any charged or neutral test particle. Then, we numerically apply these results to electrons. By studying the characteristics, we discuss the domains of initial conditions for geodesics starting inside the ergosphere. All these results come from the Kerr spacetime structure, and enhances the Penrose process as a plausible origin for the high energy jets.

**keywords:** Astrophysical jets; Kerr black hole geodesics; High energy cosmic rays

## 1 Introduction

Among the numerous observed outflows ejected from various astrophysical structures at all scales [23, 17] the longest, the most energetical and collimated jets emerge either very fugaciously and intensely from cosmological sources - like the long duration gamma ray bursts [1] -, or with lifetimes at our time scale, steadily or repeatedly, nearer, from some microquasars, or, at much larger time and space scales, from the active galaxies nuclei [25]. All of them are relativistic, and often ultra relativistic [22]. Most of these jets are believed to be powered by a central engine, being a neutron star or BH, fed by larger structures, like elliptical galaxies, giant companion stars and X-ray binaries [34]. The more and more numerous and precise [26] observations of these various jets will soon help to strongly constraint the various conjectured theoretical models. In this perspective, we are here interested to suggest a purely gravitational theoretical model of the formation of a highly energetic and collimated jet powered by a rotating BH.

As a first approximation, assuming the system to be axisymmetrical and in stationary rotation, we can represent a jet as a set of test particles following Kerr's unbound geodesics focusing at infinity along the  $z$  axis.

In this ideal framework, if we succeed to describe a perfectly collimated jet with high energies, the model will allow us to build far more realistic descriptions by taking the ambient medium, i.e. the matter (including a magnetic field), into account. However, these more realistic descriptions, although important, will only produce marginal improvements concerning the origin of the jet formation. The essential focus of the phenomenon will remain the coherent set of parallel unbound geodesics of a Kerr BH combined with the source of

powering essentially being the gravitational field in its strongest manifestations, namely the BH.

The generalized cylindrical, or Weyl, coordinates  $(\rho, z, \phi)$ , related to Boyer-Lindquist generalized spherical coordinates  $(r, \theta, \phi)$  by

$$\rho = [(r - 1)^2 - A]^{1/2} \sin \theta, \quad z = (r - 1) \cos \theta, \quad (1)$$

where

$$A = 1 - \left(\frac{a}{M}\right)^2, \quad (2)$$

are the most suitable for describing observable phenomena generated by axisymmetric structures. The existence of special unbound geodesics was recently demonstrated in this framework [14]. These geodesics stem from the ergosphere and, when  $z \rightarrow \infty$ , they are asymptotically parallel to the  $z$  axis, with

$$\rho = \rho_1 \equiv \left(\rho_e^2 + \frac{\mathcal{Q}}{E^2 - 1}\right)^{1/2} \quad (3)$$

for the asymptotes, depending on  $\rho_e \equiv a/M$  and on the two constants of motion, the Carter constant  $\mathcal{Q}$  and the energy  $E$ , the third constant of motion, the  $z$  component of the angular momentum,  $L_z$  being necessarily null. In the present paper, we show that only some of these geodesics, belonging to narrow ranges, can be followed by particles with high energies.

The function  $R(r)$  [9] introduced in the expression of the Kerr timelike geodesics (test particle mass  $\sqrt{\delta_1} = 1$ ) plays a fundamental role in the analysis of the jet collimation in the case of a model where the engine at the centre of the accretion disk is supposed to be a stationary rotating BH. This function is such that

$$R^2(r) = a_4 r^4 + a_3 r^3 + a_2 r^2 + a_1 r + a_0, \quad (4)$$

with (see (2) and (4-8) in [14])

$$\begin{aligned} a_0 &= -a^2 \mathcal{Q}, & a_1 &= 2(a^2 E^2 + \mathcal{Q}), \\ a_2 &= a^2(E^2 - 1) - \mathcal{Q}, & a_3 &= 2, & a_4 &= E^2 - 1, \end{aligned} \quad (5)$$

where we put  $M = 1$  and  $L_z = 0$ , considering the special 2D-geodesics of (3)-type. Hence, the BH spin  $a$  being fixed,  $-1 \leq a \leq 1$ , we have two independent parameters left,  $\mathcal{Q}$  and  $E$ , or, equivalently from (3), the position  $\rho_1$  of the asymptote parallel to the  $z$ -axis and the energy  $E$ .

The paper is organized as follows. In section 2, we obtain the expressions of the two motion constants,  $E$  and  $\mathcal{Q}$ , as functions of two real roots of the characteristics equation  $R^2(r) = 0$ . In section 3, we consider the special case of a double root  $Y$ , and we show that there exist only two narrow ranges of  $Y$  for which  $E$  can have high energy values. In section 4, we show that the two possible other roots are functions only of the two first ones. Then we look at some consequences on the admissible values of  $E$  and the corresponding ranges for the asymptotes  $\rho_1$ . In section 5, we calculate the energy flux of the jet, and

based on the observational evaluation of the power of the jet we deduce the corresponding particles density, the particles flow, the mean velocity and the mean Lorentz factor of the jet. As an example, we give a numerical estimation of these quantities for electrons. In section 6, by studying the characteristics, we show that among the two previous possibilities found in section 3, there remains one admissible only. In section 7, as a conclusion, we discuss qualitatively some potential consequences of relaxing some restrictive assumptions made here on the possibilities offered by the Penrose process to obtain high energies with efficient jets formation.

## 2 Conserved quantities as functions of two roots

Let us consider the possible roots of the equation  $R^2(r) = 0$  of the characteristics  $\dot{r} = 0$  of the autonomous system of geodesics equations [9], i.e.

$$a_4 r^4 + a_3 r^3 + a_2 r^2 + a_1 r + a_0 = 0. \quad (6)$$

The polynomial equation (6) has four roots, labeled  $r_i$  with  $i = 1, 2, 3, 4$ , which can be *a priori*  $\geq 0$  or  $\leq 0$  or complex (contrarily to the  $r$  physical variable which is real defined in the range  $[1 + \sqrt{A}, \infty[$ ). The two equations  $R^2(r_1) = 0$  and  $R^2(r_2) = 0$  are linear in  $\mathcal{Q}$  and in  $E^2 - 1$ . Solving the linear system of these two equations yields the two parameters as functions of the roots  $r_1$  and  $r_2$ ,

$$\mathcal{Q} = \frac{2r_1 r_2}{D} \{a^4 + a^2 [r_1(r_1 - 2) + r_2(r_2 - 2)] + r_1^2 r_2^2\}, \quad (7)$$

$$E^2 - 1 = -\frac{2}{D} \{a^4 + a^2(r_1^2 + r_2^2) + r_1 r_2 [r_1(r_2 - 2) - 2r_2]\}, \quad (8)$$

with

$$D = a^4(2 + r_1 + r_2) + a^2 [r_1^3 + r_1^2 r_2 + r_1 r_2(r_2 - 4) + r_2^3] + r_1 r_2 [(r_1^2 + r_1 r_2)(r_2 - 2) - 2r_2^2]. \quad (9)$$

In the third possible equation,  $R^2(r_3) = 0$ , the parameters  $\mathcal{Q}$  and  $E^2 - 1$  can be replaced by (7) and (8), leading to a relation between  $r_3$  and  $r_1$  and  $r_2$  allowing, in principle, to determine the values of  $r_3$  as functions of  $r_1$  and  $r_2$  only, with  $a$  being fixed. The fourth possible equation,  $R^2(r_4) = 0$ , will not bring any new result because the roots  $r_3$  and  $r_4$  are the same.

In (7) and (8), it is worth noting the symmetric role of  $r_1$  and  $r_2$ , and that  $\mathcal{Q}$  and  $E^2 - 1$  have the same denominator  $D$ , so that if, and only if, it cancels, we have  $E \rightarrow \infty$  and  $|\mathcal{Q}| \rightarrow \infty$ , whereas  $\rho_1$ , depending only on their ratio (see (3)), tends towards a finite value. From (3),(7) and (8) we obtain the asymptotes

$$\left(\frac{\rho_1}{\rho_e}\right)^2 = \frac{(a^2 + r_1^2)(a^2 - r_1 r_2)(a^2 + r_2^2)}{a^2 \{a^4 + a^2(r_1^2 + r_2^2) + r_1 r_2 [r_1(r_2 - 2) - 2r_2]\}}. \quad (10)$$

### 3 Roots $r_1 = r_2$ real

For sake of simplification, we assume in this paper that there is a double real root  $r_1 = r_2 = Y$ . Hence (4) can be rewritten as

$$R^2(r) = a_4(r - Y)^2(r^2 + Br + C), \quad (11)$$

and (7) and (8) simplify to

$$\mathcal{Q} = \frac{[a^4 + 2a^2(Y - 2)Y + Y^4]Y^2}{a^4(1 + Y) + 2a^2(Y - 1)Y^2 + (Y - 3)Y^4}, \quad (12)$$

$$E^2 - 1 = -\frac{a^4 + 2a^2Y^2 + (Y - 4)Y^3}{a^4(1 + Y) + 2a^2(Y - 1)Y^2 + (Y - 3)Y^4}. \quad (13)$$

When  $E \rightarrow \infty$ , of course,  $|Q| \rightarrow \infty$  again. But, as already noted, their ratio tends towards a finite value, so that  $\rho_1$  remains finite,

$$\left(\frac{\rho_1}{\rho_e}\right)^2 = \frac{(a^2 - Y^2)(a^2 + Y^2)^2}{a^2[a^4 + 2a^2Y^2 + (Y - 4)Y^3]}. \quad (14)$$

Choosing a "moderate" rotation of the BH, we fix  $a = M/2$  (as considered by us in [14]). Hence, we can plot the functions  $E^2 - 1 = F(Y)$  and  $(\rho_1/\rho_e)^2 = G(Y)$ , as shown in figures 1 and 2.

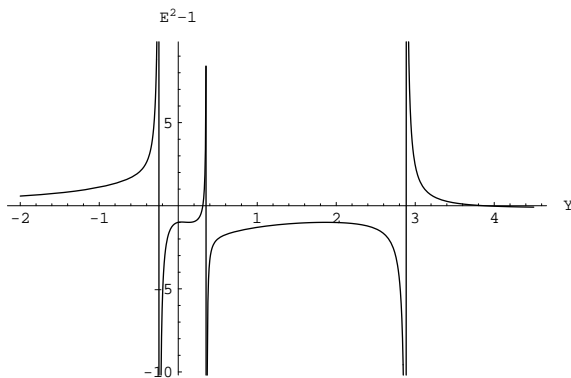


Figure 1: Plot of  $E^2 - 1 = F(Y)$ , where  $E$  is the energy of the test-particle, in function of the double root  $Y$ , evaluated from the relation (13), for a BH of mass  $M = 1$  and of angular momentum by unit of mass  $a/M = 0.5$ . We can see the ranges of  $Y$  for which  $E^2 - 1$  is positive, as expected for unbound geodesics, and the three values of  $Y$  for which  $E^2 - 1$  tends to the positive infinity.

Since  $F$  and  $G$  have to be simultaneously  $\geq 0$ , the only possible solutions correspond to the two ranges

$$Y \in [-0.5, Y_{0a}], \quad (15)$$

$$Y \in [Y_{0b}, 3.86971], \quad (16)$$

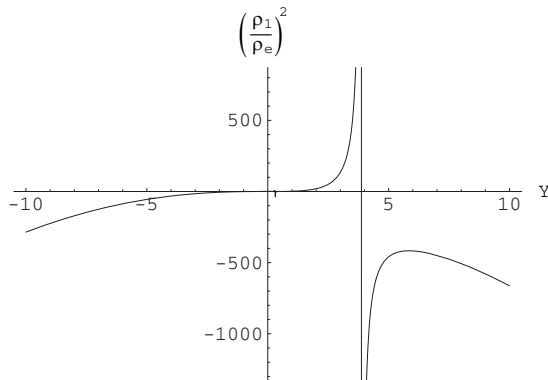


Figure 2: Plot of  $(\rho_1/\rho_e)^2 = G(Y)$  as function of the double root  $Y$ , evaluated from the relation (14), for a BH of mass  $M = 1$  and of angular momentum by unit of mass  $a/M = 0.5$ . As in figure 1, we can see the ranges of  $Y$  for which the function  $(\rho_1/\rho_e)^2$  is positive.

with  $Y_{0a}$  and  $Y_{0b}$  the asymptotes of  $F(Y)$ , for which  $E \rightarrow \infty$ . We can numerically evaluate these asymptotes (namely the roots of the equation  $D = 0$ ), yielding approximately  $Y_{0a} \simeq -0.241806$  and  $Y_{0b} \simeq 2.8832$  (for more precise values see (26) and (25) respectively).

Hence, there are two only possible values of  $\rho_1$  for which  $E \rightarrow \infty$ , i.e. one for each range (15) and (16). For the limits of the two ranges (15) and (16),  $Y = Y_{0a} - \varepsilon$  and  $Y = Y_{0b} + \varepsilon$ , when  $\varepsilon \rightarrow 0$ , we obtain the finite values, respectively,

$$\frac{\rho_1}{\rho_e} \simeq 0.693199, \quad \text{and} \quad \frac{\rho_1}{\rho_e} \simeq 10.2411. \quad (17)$$

At the other extremity of the range (16), i.e. for  $Y = 3.86971$  where  $\rho_1 \rightarrow \infty$ , we have  $E^2 - 1 = 0$ . And for the other extremity of the range (15), i.e. for  $Y = -0.5$  where  $E^2 - 1 = 2$ , we have  $\rho_1 = 0$ .

The figure 3 summarizes these results.

## 4 Roots $r_3$ and $r_4$

Identifying (11) with (4) rewritten with the parameters  $E^2 - 1 = F(Y)$  and  $(\rho_1/\rho_e)^2 = G(Y)$ , without the explicit form of these functions of  $Y$ , given by (13) and (14), yields the four relations,

$$\begin{aligned} B - 2Y &= \frac{2}{F}, \quad G + \frac{1}{F} = 2(BY^2 - 2YC), \\ 1 - G &= 16CY^2, \quad 2 - G = 4(C - 2YB + Y^2), \end{aligned} \quad (18)$$

linear in  $1/F$ ,  $G$ ,  $B$  and  $C$ .

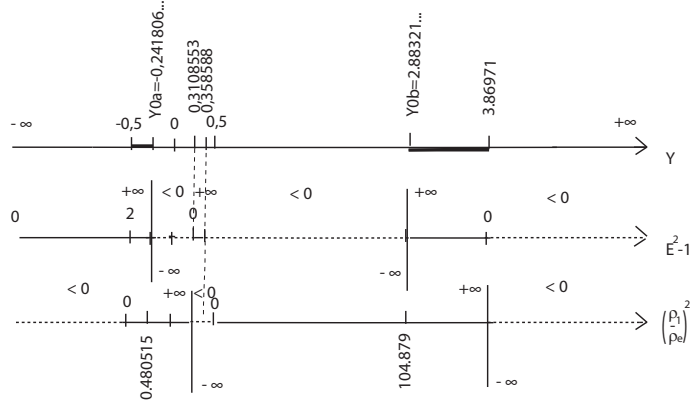


Figure 3: Some precise key values of the functions  $F(Y) = E^2 - 1$  and  $G(Y) = (\rho_1/\rho_e)^2$  showing the ranges of  $Y$  for which these functions are simultaneously positive (bold lines). The negative values of these functions are in dotted lines.

After eliminating  $1/F$  and  $G$  in (18), we obtain  $B(Y)$  and  $C(Y)$ , namely

$$B = -\frac{2(4Y^2 - 1)[Y(4Y - 1) + Y - 1]}{(4Y^2 - 1)^2 - 16Y^2(4Y - 1)}, \quad (19)$$

$$C = \frac{(4Y^2 - 1)^2 + 16Y(Y - 1)}{4[(4Y^2 - 1)^2 - 16Y^2(4Y - 1)]}. \quad (20)$$

Hence, (11) can be rewritten as

$$R^2 = a_4(r - Y)^2(r^2 - Sr + P) = a_4(r - Y)^2(r - r_3)(r - r_4), \quad (21)$$

where  $r_3$  and  $r_4$  are the remaining roots, in general distinct, and

$$S \equiv r_3 + r_4 = -B, \quad P \equiv r_3 r_4 = C, \quad (22)$$

or

$$r_3 = -\frac{1}{2} \left[ B + (B^2 - 4C)^{1/2} \right], \quad (23)$$

$$r_4 = -\frac{1}{2} \left[ B - (B^2 - 4C)^{1/2} \right], \quad (24)$$

where  $B(Y)$  and  $C(Y)$  are given by (19) and (20).

The curves  $r_3(Y)$  and  $r_4(Y)$ , are plotted in figures 4 and 5, and are real for some ranges of  $Y$  only. In particular, in the range (15) for  $Y$ ,  $r_3$  and  $r_4$  are not real. To have the expression  $r^2 + Br + C$  in Eq. (11) real, where  $B$  and

$C$  are real,  $r_3$  and  $r_4$  have to be complex conjugated, i.e.  $r_3 = z = B_1 + iC_1$  and  $r_4 = \bar{z}$ . Hence, the sign of the expression  $r^2 + Br + C = (r + B_1)^2 + C_1^2$  is always positive, and  $P = C = B_1^2 + C_1^2 \geq 0$  and  $S = -B = -2B_1 \leq 0$ .

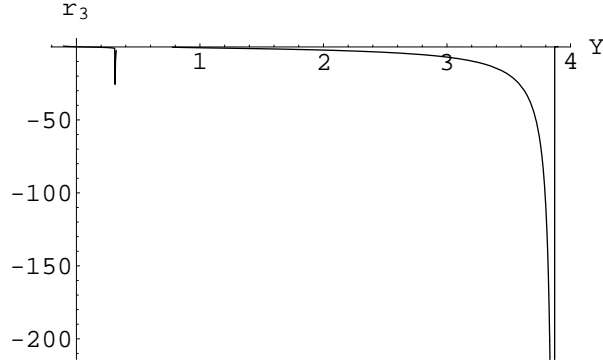


Figure 4: Plot of the root  $r_3$  in function of the double root  $Y$ , evaluated from the relation (23), for a BH of mass  $M = 1$  and of angular momentum by unit of mass  $a/M = 0.5$ .

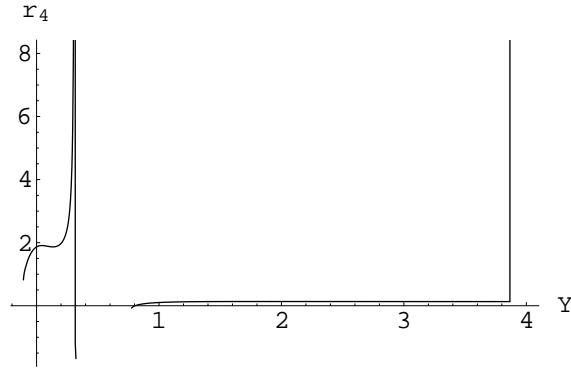


Figure 5: Plot of the root  $r_4$  in function of the double root  $Y$ , evaluated from the relation (24), for a BH of mass  $M = 1$  and of angular momentum by unit of mass  $a/M = 0.5$ .

In the range (16) for  $Y$ , the two roots  $r_3$  and  $r_4$  are real,  $P = C$  is negative (which means two roots of opposite signs) and  $B = -S$  is positive. The portions of curves  $r_3(Y)$  and  $r_4(Y)$  can be plotted on the range (16). The most precise value we can numerically obtain for the left limit (where, in principle,  $E \rightarrow \infty$ ) of the range (16), is

$$Y_{0b} \simeq 2.8832177419263523927462568785232847, \quad (25)$$



allowing us to reach the maximal value  $E \simeq 1.1 * 10^{32}$  "only". Then, the corresponding real values  $r_3 = -5.898835521038341$  and  $r_4 = 0.13240003718564175$  are obtained.

Also, it is worth observing that  $E$  is steeply decreasing, for a weak variation  $\varepsilon$  of  $Y$  from  $Y_{0b}$  ( $\varepsilon > 0$ ) or from  $Y_{0a}$  ( $\varepsilon < 0$ ), while  $\rho_1$  is weakly increasing for this same small interval of  $Y$ . For example, when  $Y$  goes from  $Y_{0b}$  to 2.922, the energy  $E$  is steeply decreasing from  $10^{30}$  to 3, while the position of the asymptote  $\rho_1/\rho_e$  increases by a small amount from 10.24 to 10.68, which means a big concentration of the most energetic part (the "spine") of the beam immediately near, at the right hand side, of  $\rho_1/\rho_e = 10.24$ . At its left hand side, there is no more beam produced.

Likewise, for the range (15), the energy  $E$  is very steeply decreasing from  $\infty$  to 6. The highest value of  $E$  ( $E_{max} \simeq 2 * 10^{30}$ ) is obtained for the most precise value numerically obtainable for the right limit  $Y_{0a}$ , namely

$$Y_{0a} \simeq -0.241805810271953623405344008301523644957. \quad (26)$$

The corresponding asymptote  $\rho_1/\rho_e$ , inside the ergosphere, decreases very slightly from 0.6932 to 0.6764. Here the jet is yet more concentrated just at the left of 0.6932. While beyond its right side, there is no possible beam.

As a result, our model predicts a radial structure of the jet, with a precise profile for its energy (or speed) distribution of the particles. A radial morphology has already been suggested from observations [15, 21].

## 5 Flux, particles density and Lorentz factor

In the region  $z \gg \rho_1$  of the jet, where the beam is quasi-parallel to the  $z$  axis, the vector density of (total) energy current is purely convective,  $\vec{j}_E = \rho_E \vec{v}$ , where  $\rho_E = n\bar{E}$ , being  $\bar{E}$  the mean energy of a particle and  $n$  is the number density,  $\vec{v} = v\vec{e}_z$  its velocity. The power of the jet or, equivalently, the energy flux across a crown, cross-section of surface  $S$ , included between two radii  $\rho_{10}$  and  $\rho_{11}$ , is

$$\begin{aligned} \mathcal{P} &= \frac{d\mathcal{E}}{dt} = \int \int_S \vec{j}_E \cdot d\vec{S} = 2\pi \int_{\bar{\rho}_{10}}^{\bar{\rho}_{11}} nv\bar{E}\bar{\rho}_1 d\bar{\rho}_1 \\ &= \pi n \int_{Y_0}^{Y_1} v\bar{E} \frac{d\bar{\rho}_1^2}{dY} dY, \end{aligned} \quad (27)$$

where  $d\vec{S} = dS\vec{e}_z$  and we supposed an homogeneous jet,  $n = \text{constant}$ . The speed of each particle is (see equation (49) of [14]),

$$v = c \left( 1 - \frac{c^4 \delta_1}{E^2} \right)^{1/2} = \frac{c}{E} (\bar{E}^2 - c^4 \delta_1)^{1/2}, \quad (28)$$

its kinetic energy is defined by

$$\bar{E}_C = (\bar{E}^2 - c^4 \delta_1)^{1/2}, \quad (29)$$

and the total energy  $\bar{E}$  is linked to the reduced function  $E(Y)$ , given in (13), by

$$E = \frac{\bar{E}}{c^2 \sqrt{\delta_1}}. \quad (30)$$

Hence we have

$$v\bar{E} = c^3(E^2 - 1)^{1/2} \sqrt{\delta_1}. \quad (31)$$

Likewise, the "true" length  $\bar{\rho}_1$  in function of the reduced coordinate  $\rho_1$ , itself function of  $Y$  by the equation (14), is

$$\rho_1 = \frac{\bar{\rho}_1}{M}. \quad (32)$$

Whence,

$$\begin{aligned} \mathcal{P} &= \frac{d\mathcal{E}}{dt} \\ &= \pi n M^2 \rho_e^2 c^3 \sqrt{\delta_1} \int_{Y_0}^{Y_1} (E^2 - 1)^{1/2} \frac{d(\rho_1/\rho_e)^2}{dY} dY, \end{aligned} \quad (33)$$

where the adimensional functions  $E(Y)$  and  $(\rho_1/\rho_e)^2(Y)$  are given by the equations (13) and (14). The relation (33) can be used to calculate, for example, the power of the beam of the particles ejected along the geodesics with asymptotes included between  $\rho_{10}/\rho_e = 0.69319914385$  and  $\rho_{11}/\rho_e = 0.676252$ , corresponding, as seen in section 4, to energies varying from the infinity (in fact,  $E \sim 2 * 10^{32}$ ) to 5.8, and with  $Y$  range (15) from  $Y_{0a} \simeq -0.241806$  to  $Y_1 = -0.250$ . However this calculation would suppose knowing the particles density  $n$  inside the jet. Conversely, if the power (which is an observational data more easily attainable by other independent methods [36, 13, 31, 32]), is known, then from our model we can deduce the density  $n$ .

Further assumptions have to be made about the ejected particles and the BH parameters. Let us consider a supermassive BH with mass  $M = 10^9 M_\odot$  (with the solar mass  $M_\odot = 3\text{km}$ ) and angular momentum by unit mass  $a = M/2$ , and electrons with restmass  $\sqrt{\delta_1} = 0.511\text{MeV}$ . Let us suppose that the jet power is  $\mathcal{P} = 10^{47}$  erg/s [36, 31]. We find with this data (the calculation can be made numerically from a series expansion of the integrant near  $Y_{0a}$ , which is justified because  $|Y - Y_{0a}| \leq |Y_1 - Y_{0a}| \simeq 8.2 * 10^{-3} < 1$ ),

$$I = \left| \int_{Y_{0a}}^{Y_1} (E^2 - 1)^{1/2} \frac{d(\rho_1/\rho_e)^2}{dY} dY \right| = 0.264939. \quad (34)$$

Whence the density is deduced

$$n = \frac{10^{47}}{8.29 * 10^{28}} = 2.18 * 10^{20} \text{ electrons/m}^3. \quad (35)$$

The flow of particles across the same crown of surface  $S$  is

$$\begin{aligned}
\frac{dN}{dt} &= n\pi \int_S v d\rho_1^2 \\
&= n\pi M^2 \rho_e^2 c \int_{Y_{0a}}^{Y_1} \left(1 - \frac{1}{E^2}\right)^{1/2} \frac{d(\rho_1/\rho_e)^2}{dY} dY \\
&= n * 3.14 * \frac{27}{4} * 10^{32} * J,
\end{aligned} \tag{36}$$

and we obtain,

$$\begin{aligned}
J &= \left| \int_{Y_{0a}}^{Y_1} \left(1 - \frac{1}{E^2}\right)^{1/2} \frac{d(\rho_1/\rho_e)^2}{dY} dY \right| \\
&= 2.30373 * 10^{-2},
\end{aligned} \tag{37}$$

and finally,

$$\frac{dN}{dt} = 1.06352 * 10^{52} \text{ electrons/s.} \tag{38}$$

From these results the mean energy by particle can be deduced,

$$\begin{aligned}
\langle \bar{E} \rangle &= \frac{d\mathcal{E}}{dt} \left( \frac{dN}{dt} \right)^{-1} \\
&= 0.511 * \frac{0.264939}{2.30373 * 10^{-2}} \simeq 5.87673 \text{ MeV/electron,}
\end{aligned} \tag{39}$$

which yields the (mean) Lorentz factor

$$\begin{aligned}
\Gamma_m \equiv \langle E \rangle &= \frac{\langle \bar{E} \rangle}{c^2 \sqrt{\delta_1}} = \frac{I}{J} = \frac{0.264939}{2.30373 * 10^{-2}} \\
&= 11.5005,
\end{aligned} \tag{40}$$

and the mean velocity

$$v_m = c \left( 1 - \frac{1}{\langle E \rangle^2} \right)^{1/2} = 0.996212 * c, \tag{41}$$

corresponding to an average ultra relativistic jet.

Now, we also can consider a narrow, more energetic, part of the jet only. As examples, let us consider the part included between  $\rho_{10}$  and  $\rho_{12} = 0.69319 * \rho_e$  (or  $\rho_{13} = 0.693199 * \rho_e$ ), corresponding to  $Y_{0a}$  and  $Y_2 = -0.24181$  (or  $Y_3 = -0.241805810272$ ), respectively, i.e. to thickness  $\delta\rho_2 = \rho_{12} - \rho_{10} = -8.68546 * 10^{-6} * \rho_e$ , for  $Y_2 - Y_{0a} = -4.18973 * 10^{-6}$  (or  $\delta\rho_3 = \rho_{13} - \rho_{10} = -9.61453 * 10^{-14} * \rho_e$ , for  $Y_3 - Y_{0a} = -4.63518 * 10^{-14}$ ), and hence to ratio of flux surfaces  $S_2/S = (\rho_{12}^2 - \rho_{10}^2)/(\rho_{11}^2 - \rho_{10}^2) = 5.18849 * 10^{-4}$  (or  $S_3/S = (\rho_{13}^2 - \rho_{10}^2)/(\rho_{11}^2 - \rho_{10}^2) = 5.74535 * 10^{-12}$ ).

Furthermore, let us (reasonably) assume that the power by unit surface crossed by the jet (i.e. the energetic flux) is constant:

$$\frac{\mathcal{P}}{S} = \frac{\mathcal{P}_i}{S_i}, \quad i = 2, 3. \quad (42)$$

Hence, the part of the jet with the thickness  $\delta\rho_2$  (or  $\delta\rho_3$ ), will have a kinetic power  $\mathcal{P}_2 = (S_2/S)\mathcal{P} = 5.18849 * 10^{43}$  erg/s (or  $\mathcal{P}_3 = (S_3/S)\mathcal{P} = 5.74534 * 10^{35}$  erg/s), a particle density  $n_2 = (S_2/S)(I/I_2)n = 4.97047 * 10^{18}$  electrons/m<sup>3</sup> (or  $n_3 = (S_3/S)(I/I_3)n = 5.23365 * 10^{14}$  electrons/m<sup>3</sup>), a flow of particles  $dN_2/dt = 1.26855 * 10^{47}$  electrons/s (or  $dN_3/dt = 1.48031 * 10^{35}$  electrons/s), a mean energy  $\langle \bar{E}_2 \rangle = \sqrt{\delta_1}(I_2/J_2)c^2 = 255.631$  MeV (or  $\langle \bar{E}_3 \rangle = \sqrt{\delta_1}(I_3/J_3)c^2 = 2.42573$  TeV), a mean velocity  $v_{m2} = 0.99999800204c$  (or  $v_{m3} = 0.99999999999778c$ ) and a Lorentz factor  $\Gamma_2 = I_2/J_2 = 500.257$  (or  $\Gamma_3 = I_3/J_3 = 4.74703 * 10^6$ ). Let us precise that  $I_2 = -6.02378 * 10^{-3}$  and  $J_2 = -1.20414 * 10^{-5}$  (or  $I_3 = -6.33485 * 10^{-7}$  and  $J_3 = -1.33449 * 10^{-13}$ ) are the integrals (34) and (37) respectively, in which the upper limit becomes  $Y_2$  (or  $Y_3$ ) instead of  $Y_1$ . So, we can see that, in its core, the jet is as more strongly UR as nearer of  $\rho_{10}$ . Let us precise that  $Y_3$ , and all the corresponding values with the index "3", corresponds to the value of  $Y$  the nearest of  $Y_{0a}$  for which we are yet able to numerically evaluate the integrals  $I_3$  and  $J_3$  (and so, the different corresponding quantities). Let us note that the conditions inside the jet for the most narrow channel we are able to evaluate are comparable to conditions inside a terrestrial particles accelerator (e.g. LHC), namely  $\langle \bar{E}_3 \rangle \sim 2$  TeV inside a channel of thickness  $\sim \delta\bar{\rho}_3 \simeq 14.4218$  cm (but here for electrons, while in the LHC there are protons. We can evaluate jets of protons as well, which would give us yet higher energies: factor  $\sim 2 * 10^3$ ). The results are summarized in the table 1.

As second example, we give the same evaluations for the second part of the very energetic jet, namely near the value  $Y_{0b} \simeq 2.88$  (25). The results are summarized in the table 2. We shall not comment more precisely these last results, because they cannot correspond to effective jets, as we shall show in the next section.

## 6 Geodesics for high energy jets

Now let us look at the possible geodesics framing a jet for values of the energy and of the corresponding asymptotes  $\rho_1$  given in section 5. The existence of admissible initial conditions for such geodesics are provided by the existence and positions of the 2D-characteristics of the system of geodesics equations (see (2) and (3) in [14]). Each characteristics curve delimits two separated parts (regions) in the plane  $(r, \theta)$  as predicted by the theory [30] often applied to the so-called "qualitative analysis". Each part contains a set of geodesics, which can never cross the characteristics towards the other part. In Boyer-Lindquist coordinates, the characteristics are defined by the equations

$$\dot{r} = 0, \quad \dot{\theta} = 0, \quad (43)$$

	$Y_1$	$Y_2$	$Y_3$
$Y$	-0.250	-0.24181	-0.241805810272
$Y - Y_{0a}$	$-8.19419 * 10^{-3}$	$-4.18973 * 10^{-6}$	$-4.63518 * 10^{-14}$
$E$	5.81378	250.13	$2.37778 * 10^6$
$\delta\rho_i/\rho_e$	-0.0169469	$-8.68546 * 10^{-6}$	$-9.61453 * 10^{-14}$
$\delta\rho_i (m)$	$2.54204 * 10^{10}$	$1.30282 * 10^7$	$14.4218 * 10^{-2}$
$P (erg/s)$	$10^{47}$	$5.18849 * 10^{43}$	$5.74534 * 10^{35}$
$I$	-0.264939	$-6.02378 * 10^{-3}$	$-6.33485 * 10^{-7}$
$n (e^-/m^3)$	$-2.18711 * 10^{20}$	$-4.97047 * 10^{18}$	$5.23365 * 10^{14}$
$J$	$-2.30373 * 10^{-2}$	$-1.20414 * 10^{-5}$	$-1.33449 * 10^{-13}$
$dN/dt (e^-/s)$	$1.06352 * 10^{52}$	$1.26855 * 10^{47}$	$1.48031 * 10^{35}$
$E_m (Mev)$	5.87673	255.631	$2.42573 * 10^6$
$1 - v_m/c$	$3.788 * 10^{-3}$	$1.99796 * 10^{-6}$	$2.22 * 10^{-14}$
$\Gamma$	11.5005	500.257	$4.74703 * 10^6$

Table 1: Values of the departures of the position from the asymptotes at high energies, the thickness of the jet, its density, its mean energy, its mean velocity and its (mean) Lorentz factor, as function of the parameter  $Y$ , for  $Y$  in the vicinity of  $Y_{0a}$  (26), where  $E \rightarrow \infty$  and  $\rho_1/\rho_e \rightarrow 10.24106$  ( $E_{max} = 1.1 * 10^{32}$ ). The integrals  $I$  and  $J$  are defined by (34) and (37) with the corresponding upper limit  $Y_i$  ( $i = 1, 2, 3$ ), the lower limit being  $Y_{0a}$ .

which are equivalent, from equations (19) and (20) in [14], to the system of algebraic equations,

$$P = 0, \quad S = 0, \quad (44)$$

the solutions of which, when they exist, are some values of  $r_i$  of  $r$  (previously introduced in Sections (2) to (4)) and some values  $\theta_i$  of  $\theta$ , respectively (which define circles and straight lines from the origin respectively).

In Weyl coordinates,  $\rho$  and  $z$ , these characteristics equations (44) are equivalent to the equations (see (17) and (18) in [14])

$$\dot{\rho} = \frac{S(\alpha^2 - A)z}{\alpha\rho\Delta}, \quad \dot{z} = -\frac{S\alpha}{\Delta}, \quad (45)$$

and

$$\dot{\rho} = \frac{P\alpha^3\rho}{(\alpha^2 - A)\Delta}, \quad \dot{z} = \frac{P\alpha z}{\Delta}, \quad (46)$$

respectively, where

$$\Delta = (\alpha + 1)^2\alpha^2 + \left(\frac{a}{M}\right)^2 z^2. \quad (47)$$

Each set of equations (45) and (46) lead to,

$$\frac{dz}{d\rho} = -\frac{\alpha^2\rho}{(\alpha^2 - A)z}, \quad (48)$$

	$Y_1$	$Y_2$	$Y_3$	$Y_4$
$Y$	2.922	2.833	2.88321774193	2.883217741926354
$Y - Y_{0b}$	$3.87823 * 10^{-2}$	$8.2258 * 10^{-5}$	$3.6473 * 10^{-12}$	$1.33227 * 10^{-15}$
$E$	3.027	63.7027	302514	$1.50555 * 10^7$
$\delta\rho_i/\rho_e$	0.411539	$8.49897 * 10^{-4}$	$3.76801 * 10^{-11}$	$1.77636 * 10^{-14}$
$\delta\rho_i$ (m)	$6.17309 * 10^{11}$	$1.27485 * 10^9$	56.5201	$2.66454 * 10^{-2}$
$P$ (erg/s)	$10^{47}$	$2.02457 * 10^{44}$	$8.97533 * 10^{36}$	$3.96648 * 10^{33}$
$I$	49.1803	2.21766	$4.668989 * 10^{-4}$	$7.2287 * 10^{-6}$
$n$ ( $e^-/m^3$ )	$1.17177 * 10^{18}$	$5.26106 * 10^{16}$	$1.10759 * 10^{13}$	$3.16214 * 10^{11}$
$J$	8.33589	$1.74073 * 10^{-2}$	$7.62157 * 10^{-10}$	$3.63748 * 10^{-12}$
$dN/dt$ ( $e^-/s$ )	$2.07028 * 10^{52}$	$1.94106 * 10^{48}$	$1.78919 * 10^{37}$	$2.43823 * 10^{33}$
$E_m$ (Mev)	3.01481	65.1005	313 100	$1.01536 * 10^6$
$1 - v_m/c$	$1.4469 * 10^{-2}$	$3.1 * 10^{-5}$	$1.3318 * 10^{-12}$	$1.266 * 10^{-13}$
$\Gamma$	5.89983	127.398	612 719	$1.98701 * 10^6$

Table 2: Same values as table 1 but in the vicinity of  $Y_{0b}$  (25) where  $E \rightarrow \infty$  ( $E_{max} = 2 * 10^{30}$ ) and  $\rho_1/\rho_e \simeq 0.69$ .

and

$$\frac{dz}{d\rho} = \frac{(\alpha^2 - A)z}{\alpha^2\rho}, \quad (49)$$

respectively, defining the two families of characteristics for the geodesics of type (21) in [14] in which we are interested, namely, ellipses (corresponding to  $\dot{r} = 0$ ) and hyperboles (corresponding to  $\dot{\theta} = 0$ ). Let us note that the product of the two derivatives (48) and (49) of these characteristics is  $-1$  (which confirms that they are orthogonal).

The first ones, ellipses, exist when there are solutions  $r = r_i = \text{constant}$  of (48) for  $\forall\theta$ , with  $r_i \geq 1 + \sqrt{A}$  or equivalently  $\alpha = \alpha_i = \text{constant}$  ( because  $\alpha = r - 1$ ) with  $\alpha_i \geq \sqrt{A}$ . Then (48) can be integrated yielding

$$\left(\frac{z}{\alpha_i}\right)^2 + \frac{\rho^2}{\alpha_i^2 - A} = K_1, \quad (50)$$

where  $K_1$  is an integration constant. Comparing (50) with the equation (12) of [14] imposes  $K_1 = 1$ .

The second ones, hyperboles, exist when there exist solutions  $\mu = \mu_i = \text{constant}$  of (49) for any  $r$ , with  $\mu_i^2 \leq 1$ . These are solutions of the equation  $S = 0$ , when  $L_z = 0$ , with

$$S^2 = \left(\frac{a}{M}\right)^2 (E^2 - 1)\alpha^4 \left[1 - \left(\frac{z}{\alpha}\right)^2\right] \left[\frac{\mathcal{Q}}{a^2(E^2 - 1)} + \left(\frac{z}{\alpha}\right)^2\right]. \quad (51)$$

There are two possible cases, namely  $\mu_i^2 = 1$ , then  $S = 0$  for any  $\mathcal{Q}$ , or  $\mu_i^2 = -\mathcal{Q}/[a^2(E^2 - 1)] = 1 - (\rho_1/\rho_e)^2 \leq 1$ , being positive defined only if  $\mathcal{Q} \leq 0$ , or equivalently, if  $\rho_1 \leq \rho_e$ . Then, for  $\mu_i^2 = 1$ , we have  $z = r - 1 = \alpha$  and  $\rho = 0$  for any  $r$  and (49) reduces to  $\rightarrow \infty$ , and the characteristics being along the semi-axis  $z \geq \sqrt{A}$ . While for  $\mu_i^2 = -\mathcal{Q}/[a^2(E^2 - 1)]$  we have for (49)

$$\frac{dz}{d\rho} = \frac{z^2 - A\mu_i^2}{z\rho}, \quad (52)$$

which can be integrated leading to

$$\rho = K_2 \left[ \left( \frac{z}{\mu_i} \right)^2 - A \right]^{1/2}, \quad (53)$$

where  $K_2$  is an integration constant. Comparing (53) with (12) in [14] we have  $K_2 + \mu_i^2 = 1$ .

The expression (53) represents a family of hyperboles parametrized by

$$\frac{\rho_1}{\rho_e} = (1 - \mu_i^2)^{1/2}, \quad (54)$$

yielding

$$\frac{1}{A} \left[ 1 - \left( \frac{\rho_1}{\rho_e} \right)^2 \right]^{-1} z^2 - \frac{1}{A} \left( \frac{\rho_1}{\rho_e} \right)^{-2} \rho^2 = 1. \quad (55)$$

If the initial condition (IC) of a geodesics lies inside an ellipse of the type (50), this geodesics cannot be an unbounded geodesics, and hence cannot go to infinity. So, the admissible IC have to satisfy the triple condition: i) being inside the ergosphere, in order to be possibly issued from a Penrose process; ii) being outside the larger elliptic characteristics, this means corresponding to the larger value of the roots  $r_i$ ; and iii) being above the higher hyperbolic characteristics, which corresponds to the higher values of the roots  $|\mu_i| \leq 1$ . That restricts the admissible domain of IC.

An ellipse (50), when it exists (i.e. when  $r_i \in [1 + \sqrt{A}, \infty[$ ), can intersect the ergosphere only if its semi-minor axis  $b_i = (\alpha_i^2 - A)^{1/2}$  is smaller than  $\rho_e = a/M$ , i.e. if  $r_i < 2$ .

As example, let us take the special case of a double root  $Y$  studied in the precedent sections.

a) The first admissible range that we found is  $Y \in [Y_{0b}, 3.86]$  (see figure 3). These roots, belonging to the domain of physical definition,  $r \in [1 + \sqrt{A} = 1.86, \infty[$ , all correspond to the existence of elliptic characteristics. The smallest ellipse has as semi-minor axis  $b_i = [(Y - 1)^2 - A]^{1/2} = [(1.88)^2 - 0.75]^{1/2} = (2.78844)^{1/2}$  along  $\rho$ , and as semi-major axis  $a_i = \sqrt{\alpha_i^2} = Y - 1 = 1.88$  along  $z$ , obtained for the smallest value  $Y_{0b} \simeq 2.88$ , corresponding to  $\rho_1/\rho_e \simeq 10.24$ . This ellipse contains the ergosphere, the limits of which being  $z_{\max} = \sqrt{A} = 0.866025$  and  $\rho_{\max} = 1/2$ . Hence, it is always impossible to have IC simultaneously inside the ergosphere and outside any ellipse. There is no possibility of unbound geodesics starting from the ergosphere in this first case.

b) For the second admissible range we found that  $Y \in [-0.5, Y_{0a}]$  (see figure 3). These roots do not belong to the domain of definition of the physical variable  $r$ , which means that there are never any corresponding elliptic characteristics. The only remaining possible limitation depends on the position of the hyperbolic characteristics (55). The hyperbola intersects the  $z$ -axis at the point with coordinates  $\rho = 0$  and  $z_0 = \{A[1 - (\rho_1/\rho_e)^2]\}^{1/2}$  and tends asymptotically towards

the straight line of equation  $\rho \simeq z \tan \theta_1$ , with  $\sin \theta_1 = \rho_1/\rho_e$ . The domain of possible IC is located between the  $z$ -axis, the limit of the ergosphere and above the hyperbola. For example, for  $Y = -0.241806$ ,  $\rho_1/\rho_e = 0.693199$ ,  $\theta_1 = 21^\circ$ , and  $z_0 = 0.624185 (< \sqrt{A} = 0.8660254037844386)$ . We plot in figure 6 the geodesics which tends asymptotically towards the corresponding  $\rho = \rho_1 = 0.3466$ , for which the test particle has a very high (theoretically infinite) energy (for the calculations, we choose the value  $E = 10^6$  and  $\rho_1/\rho_e = 0.693199$ ). This plot corresponds to the IC  $\rho_i = 2.8 * 10^{-6}$  and  $z_i = 0.852086186870110$  which are (just) inside the ergosphere at its top near the  $z$ -axis, i.e. near the event horizon. For the other limit,  $Y = -0.5$ , of the  $Y$  range,  $\rho_1 = 0$ ,  $E = \sqrt{3}$ ,  $\theta_1 = 0$  and  $z_0 = \sqrt{A} = 0.866$ .

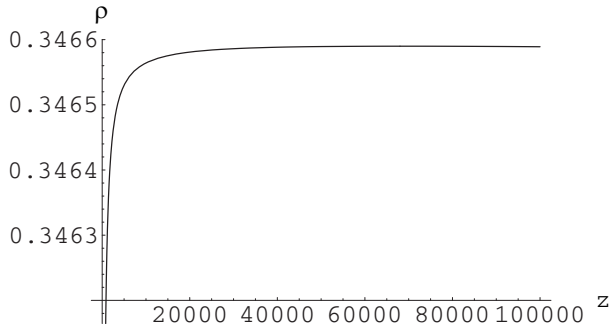


Figure 6: Plot of the geodesics  $\rho(z)$ , for the parameters  $a = 0.5M$  and  $M = 1$  of the BH, the motion constants  $L_z = 0$ ,  $E = 10^6$ ,  $\mathcal{Q} = [(\rho_1/\rho_e) - 1](E^2 - 1)(a/M)^2$  (with  $\rho_1/\rho_e = 0.693199$ ) of the test-particle, and for the initial conditions  $\rho_i = 2.8 * 10^{-6}$ ,  $z_i = 0.852086186870110$ , inside the ergosphere. We can observe that this geodesics is asymptotically parallel to the  $z$ -axis at the asymptote of equation  $\rho = \rho_1 \equiv 0.3466$ , at least until the altitude  $z \simeq 8 * 10^4$ . For a greater altitude, a greater precision on the initial conditions would be necessary, theoretically without any limitation.

## 7 Discussion

Taking as parameters the roots of a characteristics equation for unbound 2D-geodesics with  $L_z = 0$ , we showed that the two remaining motion constants,  $E$  and  $\mathcal{Q}$ , of a test particle following geodesics which asymptotically tends towards a parallel line to the  $z$ -axis, can be deduced as a function of these parameters. In the special case of a double root, and choosing the BH angular momentum by unit of mass  $a = M/2$ , restricted domains of  $\rho_1$  asymptotes corresponding to high energies are found. That means that the Kerr metric can generate powerful collimated jets in some precise regions only (and, as a consequence, from some precise regions of the ergosphere). Indeed, we obtained, in this special case, two only possible ranges of  $\rho_1$ , namely  $\rho_1 \in [0.3382, 0.3466]$  and  $\rho_1 \in [5.12, 5.34]$



for  $E \in [\sqrt{6}, \infty[$  and  $E \in ]\infty, \sqrt{3}]$  respectively (see the figure 3). Then, for electrons, we calculated the particle density, the particle flow, the thickness of the jet and the Lorentz factor, exhibiting UR jets. The numerical evaluations were summarized in the tables 1 and 2.

These results can be pertinent both for jets and for ultra high energy cosmic rays (UHECR). Indeed, such energies can be obtained with quasi unlimitedly values inside the ergosphere thanks to the Penrose process. That comes from the fact that this process implements three levels (orders of magnitude) of rest masses (or of energies): the BH mass (which could be designated as a "super-macroscopic", or astrophysical mass), the incident mass of the body going into the ergosphere along the equatorial plane from the accretion disk (which could be called a "macroscopic" mass); and the particle going out of the ergosphere asymptotically parallel to the  $z$  axis (which could be called a "microscopic" mass).

The "microscopic" outgoing particle, via the original Penrose process [27], simply by its separation from the incident macroscopic body inside the ergosphere, can acquire a kinetic energy of order of magnitude of this ingoing mass, i.e. a "macroscopic" kinetic energy.

The simplest example of such a process could be the ionization of an ingoing atom of hydrogen inside the ergosphere, with its nucleus irreversibly falling into the event horizon while the electron is ejected along a geodesic asymptotically to  $\rho_1$  with a kinetic energy increased of about 1836 times its rest mass. The rest mass of the nucleus (the proton) could be considered as the lowest limit of a macroscopic body, being in this case the electron the microscopic particle.

If the principle of this phenomenon, for the formation of UHECR in collimated jets, is realistic, we have to expect the total mass of the ingoing body to be "macroscopic" as compared to (i.e. infinitely larger than) the total mass of the ejected particles, and to be of the same order of magnitude than the mass falling in the BH after each Penrose type decay inside the ergosphere.

Then, in terms of "rest mass" (i.e. of the amount of matter), the efficiency of the Penrose process is very (infinitely) weak, meaning that a very weak part of the ingoing mass is ejected to the outside. But in terms of energy (a conserved quantity), the Penrose process is very (infinitely) efficient, meaning that the energy of the ejected particles is much (infinitely) larger than the energy of these same incident microscopic particles (when they were linked yet to the incident macroscopic body).

We can make an analogy with a "superelastic" shock, as sometimes occurs in nuclear physics, in which the total kinetic energy of the final outgoing particles is greater than the kinetic energy of the initial ingoing particles, the difference being acquired to the detriment of a part of the ingoing (rest) mass, called "mass defect" (as opposed to an "elastic shock", for which the kinetic energy is conserved, or to an "inelastic shock" for which the final kinetic energy is lower than the initial one). In our case, the lost mass falling into the BH is equivalent to the "mass defect", and is found again in the form of kinetic energy of the ejected mass. Besides, the efficiency of a collimated jet formation (in terms of mass as well as of energy) is apparently even more weakened by the fact

that, on the set of ejected particles (in all the directions from the ergosphere, by this process), very few are ejected in a direction which is asymptotically parallel to the  $z$ -axis [24]. However, the only possible collimation being in this direction, the coherent set of these particles gives them a privileged observable character, which does not exist for the other particles isolatedly scattered in all the directions.

Recent results of the Pierre Auger Observatory [33] seem to show a correlation between the UHECR (above 57EeV) and the nearby ( $< 71$  Mpc) AGNs. It would be interesting to examine more precisely the correlations with the directions (radioloud, quasars or blazars) of the jets and with the proximity of their sources.

All the results, up to the section 4 (in particular the numerical values, which concern adimensional quantities), are strict consequences of the structure of the Kerr metric where we solely fixed the BH spin,  $a = M/2$ , and we made the assumption of a double real root  $Y$ .

A first expected position of the asymptote corresponding to an "infinite" energy in our model is  $\rho_1 \simeq 10\rho_e = 5M = 2.5 * r_S$ . The second asymptote predicted by our model for a very high energy is  $\rho_1 = (0.693199/2)M \simeq 0.3466M$ , i.e. at about 1/6 of the Schwarzschild radius  $r_S = 2M$ . This last case is the only compatible with the limitations imposed by the characteristics of the system of geodesics equations, as seen in section 6. That means that the presently described jet is a very thin (narrow) jet.

Besides, there will be a strong concentration of the most energetic part of the beam in the close vicinity of these two asymptotes, with, on one side, an abrupt (steep) decreasing and, on the other side, a smoother decreasing, which indicate a radial energetic structure of the jet, as observed [15].

The rarity of the currently detected UHECR [3] could be explained in our model by the rarity of UHE particles in the very narrow beams near the two asymptotes shaping the jet, i.e. directly observable in the very precise axial direction only. Even though the energies have to be limited ( $< 50EeV$ ) by the Greisen-Zatsepin-Kuzmin effect, firstly primary particles with energies  $< 50EeV$  could come from nearby ( $< 70$  Mpc) AGN to the earth (principally neutrinos), and secondly, for more energetic and more distant primary particles, a particular mechanism, for instance with secondary particles, can be considered [12]. Anyway, the recent observations of multi-TeV photons from distant blazars which do not display the expected spectrum (with suppressions due to the interaction with the cosmic microwave background) require an explanation [4].

Let us briefly recall that we found these results under some restrictive conditions, taken into account in section 3, especially the assumption of the existence of a double root  $Y$ , and the choice of the "middle" value  $a = M/2$ . We can thus hope that by "relaxing" these assumptions, other more general results could emerge.

For instance, relaxing the assumption of a double root  $Y$ , while keeping the same value  $M/2$  of the parameter  $a$ , could open the possibility of other solutions with  $\rho_1 > \rho_e$ , i.e. thicker jets, for admissible high energy jets. Work is

in progress in that way and our first results are encouraging. Another example could be to study, in this model, the role of the BH spin  $a$  by trying (say) higher values of this parameter. Let us note, by the way, that there are few observational results concerning the possible values of  $a$  [37, 20, 5, 6], and its possible correlation with the length and power of the jet, while there are more numerous observations concerning the values of  $M$ .

Our results can also easily be extended to particles other than electrons, for example to protons or neutrinos. This does not change the "geometry" that we obtained, i.e. the positions  $\rho_1$  of the jets, but their energy only.

For a proton ( $\sqrt{\delta_1} \simeq 1\text{GeV}$ ) the maximal energy we can here numerically calculate (but which is theoretically as large as we want) is about  $E \simeq 5.6 * 10^{25} eV = 5.6 * 10^7 EeV$ , which largely includes the highest energies of the current observed UHECR [3, 10, 19].

Finally, let us also recall that our model does not require magnetic fields, which allows us to discard some problems related to their strength [11], necessary to obtain such huge energies, and permits us to consider neutral particles as well. For example, a neutrino, which mass is assumed to be  $\sqrt{\delta_1} = 0.33eV$  [35], for the precedent evaluation, would reach the energy  $E \simeq 2 * 10^{-2} EeV$ , which seems to be an acceptable value [16, 19, 8].

In our model, the only role played by a magnetic field is the role of the induced magnetic field which tends to stabilize the jet (e.g. [2, 21]). The inner part of the parallel jet, if composed for instance of electrons only, creates a magnetic field, which tends to stabilize the collimation for its outer part (which is the most energetic part in the precedent example  $\rho_1 = 0.3466M$ ). The strength of the magnetic field depends on the relative part of the charged particles in the jet. The radial structure of the jet, in our model, supported by direct observations [15], would require a stability study. However, a first rough evaluation shows that the ratio  $\sqrt{\delta_1}/E_C \simeq \sqrt{\delta_1}/E$  remains always  $\ll 1$  inside the UR jet, which let us think that any Kelvin-Helmholtz instability is negligible, in accordance with the results of extensive studies in 2D [28] or in 3D [29].

Recent articles discussed the possibility to generate high energy particles by collisions near a BH [18] and evoked the interest to consider the Penrose process [7]. Our approach can be seen as a contribution to this debate.

## References

- [1] Aielli, G., Bacci, C., Bartoli, B., et al. 2009, *Astropart. Phys.*, 32, 47
- [2] Appl, S. & Camenzind, M. 1992, *A&A*, 256, 354
- [3] Auger Collaboration. 2007, arXiv:astro-ph/0711.2256v1
- [4] Aharonian, F., Akhperjanian, A. G., Bazer-Bachi, A. R., et al. 2006, *Nature*, 440, 1018
- [5] Aschenbach, B., Grosso, N., Porquet, D. & Predehl, P. 2004, *A&A*, 417, 71

- [6] Aschenbach, B. 2009, arXiv:astro-ph.HE/0911.2431v1
- [7] Bañados, M., Hassanain, B., Silk, J. & West, M. 2010, arXiv :1010.2724v1 [astro-ph.CO]
- [8] Berezhinsky, V., Gazizov, A., KachelrieB, M. & Ostapchenko, S. 2010, arXiv:astro-ph.HE/1003.1496v2
- [9] Chandrasekhar, S. 1983, *The Mathematical Theory of Black Holes* (Oxford: Oxford University Press) p. 346
- [10] Dermer, C. D., Razaque, S., Finke, J. D. & Atoyan, A. 2009, *New J.Phys.*, 11, 065016
- [11] de Souza, R. S. & Opher, R. 2010, *JCAP*, 02, 022
- [12] Essey, W. & Kusenko, A. 2010, *Astropart. Phys.*, 33, 81
- [13] Fender, R. P., Belloni, T. M., & Gallo, E. 2004, *MNRAS*, 355, 1105
- [14] Gariel, J., MacCallum, M. A. H., Marcilhacy, G., & Santos, N. O. 2010, *A&A*, 515, A15
- [15] Giroletti, M., Giovannini, G., Feretti, L., et al. 2004, *ApJ*, 600, 127
- [16] Gorham, P. W., Allison, P., Baughman, B. M. et. al. 2010, arXiv:astro-ph.HE/1003.2961v2
- [17] de Gouveia Dal Pino, E. M. 2005, *Advances in Space Research*, 35, 908
- [18] Grib, A.A. and Pavlov, Y.V. 2010, arXiv:1001.075v1 [gr-qc]
- [19] Hoover, S., Nam, J., Gorham, P. W., et al. 2010 arXiv:astro-ph.HE/1005.0035v2
- [20] Istomin, Ya. N. 2004, *New Astron.*, 10, 157
- [21] Keppens, R., Meliani, Z., van der Holst, B. & Casse, F. 2008, *A&A*, 486, 663
- [22] Königl, A. 2010, *IJMPD*, Vol. 19, No6, pp. 635-647
- [23] Levinson, A. 2010, *IJMPD*, Vol.19, No6, pp.649-657
- [24] Metzger, B. D. 2010, arXiv:astro-ph.HE/1001.5046v1
- [25] Mirabel, I. F. 2004, arXiv:astro-ph/0405.433v1
- [26] Müller, C., Kadler, M., Ojha, R., et al. 2010, arXiv:astro-ph.CO/1005.2626v1
- [27] Penrose, R. 1969, *Rivista del Nuovo Cimento*, numero special 1, 252

- [28] Perucho, M., Marti, J. M., Cela, J. M. & Hanasz, M. 2005, *A&A*, 443, 863
- [29] Perucho, M., Marti, J. M., Hanasz, M., de la Cruz, R. & Rubio, F. 2010, [arXiv:astro-ph.HE/1005.4332v1](https://arxiv.org/abs/astro-ph/1005.4332v1)
- [30] Pontriaguine, L. 1975, *Equations Differentielles Ordinaires* (Moscow: Mir)
- [31] Punsly, B. 1999a, *ApJ*, 527, 609
- [32] Punsly, B. 1999b, *ApJ*, 527, 624
- [33] Roulet, E. & the Pierre Auger Collaboration. 2009, *Nucl. Phys B*, 190, 169
- [34] Russel, D. M., & Fender, R. P. 2010, *Powerful Jets from Accreting Black Holes: Evidence from the Optical and Infrared in Black Hole and Galaxy Formation* (Nova Science Publishers, Inc.) and [arXiv:astro-ph.HE/1001.1244v1](https://arxiv.org/abs/astro-ph/1001.1244v1)
- [35] Steidl, M. 2009, [arXiv:nucl-ex/0906.0454v1](https://arxiv.org/abs/nucl-ex/0906.0454v1)
- [36] Willott, C., Rawlings, S., Blundell, K., & Lacy, M. 1999, *MNRAS*, 309, 1017
- [37] Zhang, S. N., Cui, W. & Chen, W. 1997, *ApJ*, 482, L155